Zeolite-supported catalysts for CO_2 methanation: The influence of transition metals incorporation in the performances

Diogo Canastreiro, nº 87385

Abstract

Aiming to improve the activity of zeolite-based catalysts for the carbon dioxide methanation reaction, a study was performed on the incorporation of several (Fe, Ni, Co and Cu) transition metals on those same supports. On the first set of catalytic tests, nickel proved to be the most active added metal, hence a second study on which metal would be the best promoter was carried out, so a series of bimetallic catalysts were developed (15Ni1Fe, 15Ni1Co and 15Ni1Cu). The most active catalyst was the iron-promoted. Hence, a third study upon which content of iron would be ideal was performed and three catalysts (15Ni1Fe, 15Ni2Fe, 15Ni3Fe) were compared. For low temperatures, 15Ni2Fe obtained better results, whilst for higher temperatures (and in an overall range of temperature), 15Ni1Fe proved to be the most active catalyst, with its highest value for CO_2 conversion of 71,5% and CH_4 selectivity of 98,25% at 350ºC.

Keywords

CO_2 Methanation; Transition Metals; Power-to-Gas; Zeolites; Thermal Catalysis.

Introduction

CO_2 continues to be the main threat for humanity's longevity, caused by its own naivety and inertia.

According to the Intergovernmental Panel on Climate Change (IPCC) [5], the best mitigation scenarios require the availability and widespread deployment of bioenergy with carbon dioxide capture and storage (BECCS). This means that without a good method of converting the CO_2, it would be impractical to just capture it through DAC. It's hard to define the exact number for the cost of removing one ton of carbon from the air, however it has been established as at least 170 € [4]. Multiplying this value with the total amount of emissions would result in loss of 8,7 trillion € yearly. In other words, using the DAC system to solve the carbon problem would consume approximately 12,1 % of the world's economy every year. Hence, at the current rate, it would be quite impossible to perform DAC on all this carbon dioxide.

Although worrisome when released in the atmosphere, carbon dioxide could also be our saviour, by being a desired feedstock for a multitude of processes, from which many useful value-added chemicals can be made.[8] The main reaction to convert CO_2 into a valuable chemical is the Sabatier reaction, which converts carbon dioxide into methane ($CO_2 + 4H_2 \rightarrow CH_4 + 2H_2O$).

H_2 production has of yet still many issues, such as storage and transport. One possible solution to these problems involves its storage and transportation as value-added compounds. Thus, the conversion of carbon dioxide and hydrogen to methane promises not only to solve the fixation of CO_2 problem, but also the H_2 storage and transport problem.

The catalytic hydrogenation of CO_2 to methane is usually performed over relatively high temperatures (250 to 400 ºC), over certain metals such as Ni and Ru, supported over silica or alumina, and under atmospheric or relatively moderate pressures. It is a highly exothermic, however thermodynamically favourable reaction. Many catalysts have been tested towards this process, and in general, noble metals have high efficiencies, and produce almost exclusively methane, however their prices make their widespread use in industrial scale impracticable. For that reason, Ni-based catalysts have been the most widely used and studied, for their high activity and selectivity towards methane, as well as for its low price and widespread availability.

Since transition metals have also been obtaining very interesting results [7], a study upon some of the cheapest and highly active elements of said group was performed. In addition, the zeolites have also been getting a lot of attention [1][2][3][6], and since Ni-doped USY catalysts have reported higher stabilities [1][2], while maintaining the thermal catalytic activity, a study combining these two factors was developed.

Experimental Section

Catalysts preparation and characterization

The catalysts have as starting material the CBV 780 zeolite from *Zeolyst International*,

comprising a HUSY zeolite (acid form of the USY zeolite, <0,02% wt of Na), containing an Si/Al ratio of 38. This compound was mixed with a solution of $CsNO_3$ (1M) and stirred for 4h at room temperature. Three ion exchanges were performed, intermixed with filtration and washing with distilled water until a pH of 7 was obtained, followed by a drying at 100 °C overnight. Each support thus contains around 1,5 %wt of cesium, corresponding to an exchange degree of 34%, thus one third of the negative charges are being compensated by the Cs^+, and the remaining two thirds by H^+. Afterwards it followed a calcination of the dried sample, performed in two steps, first at 200 °C for 1h, then at 500 °C for 6h, respectively, for an air flow of 60 ml min^{-1} $g_{zeolite}^{-1}$ and a heating rate of 2 °C/min.

For the first study, four monometallic samples were prepared by impregnation of 15 %wt of Ni, Cu, Co or Fe over the referred zeolite, following a 15X format. For the second study, catalysts containing 15 %wt of Ni and 1% of Co, Cu or Fe were prepared through co-impregnation (15Ni1X). Whilst for the third, it followed the format 15NixFe, where the co-impregnation method was followed, solely varying the iron content. These were dried overnight at 100ºC, and afterwards calcined by a temperature program from room temperature to 500ºC, at a heating rate of 2,5ºC/min, and then maintained at 500ºC for 11h.

The crystalline structure of samples was evaluated through X-Ray Diffraction using a *Bruker AXS Advance D8* diffractometer, which utilised Cu Kα radiation, and operated at 40 kV and 40 mA. For the present study, the major focus of XRD was to determine the average particle size, as well as to identify any damage that may have been done to the zeolite's structure after the metal's impregnation. Two distinct 2θ ranges were evaluated (first from 0.7 to 2.5°, with a step of 0.03 every 4 seconds, and second from 5 to 80° with a step size of 0.03/2s), in order to better identify the mesoporous structure as well as the different oxides present in the calcined samples. In addition, the spent samples were also analysed in order to evaluate the integrity of the material's structure after reaction.

Temperature programmed reduction (TPR-H_2) studies utilising hydrogen were performed on the *Autochem II* equipment from *Micromeritics*. All the samples were tested according with the same following conditions: the pre-treatment was performed at 250ºC using argon as inert gas. After cooling until 20ºC, the TPR developed with the presence of a flow of 95% argon and 5% H_2, until 900ºC, with a heating rate of 10ºC/min. The hydrogen consumed was controlled by a TCD detector.

Thermogravimetric analysis (TGA) of the samples was performed on a *Setsys Evolution TGA* machine, from *Setaram Instruments,* from 20 up to 400 ºC, at a heating rate of 10ºC/min. Under a gaseous air flow of 30 mL/min.

The microstructure of the samples was studied through Transmission Electron Microscopy (TEM), which was performed using a *HRTEM 2010 JEOL LaB6* microscope (200kV).

Specific surface areas were obtained through N_2 adsorption measurements which were carried out at -196ºC on an *Autosorb iQ* equipment from *Quantachrome.* Before adsorption, the samples were degassed in vacuum (90ºC for 1h, followed by 350ºC for 4h).

Catalytic Tests

Catalytic tests were performed at atmospheric pressure, using a constant mass for all catalysts of 0.200g, with an inlet flow of 287 ml/min, which is the optimized gaseous inflow for the present operational setup, intended to avoid any external diffusion limitations. The feed gas molar composition ratio corresponds to $CO_2/H_2/N_2$ = 9/36/10. These tests were conducted from 200°C to 450°C.

Samples were reduced from room temperature to 470 °C, with a heating rate of 2,5°C/min, and then maintained at 470°C for 1h with a molar percentage of 80 %H_2 and 20%N_2 for a flow of 250mL/min.

Water present in the outlet of the reactor was removed using an ice trap prior to the analysis performed by the detectors. The concentrations of CO_2 and CO were measured through infrared detectors, whilst methane's concentration was determined through gas chromatograph, so that molar flow rates can be measured and used for the calculation of the conversion.

Results and discussion

First Study: Effect of the Metal Nature

Catalyst's characterization

Through the observation of Fig. 1, the H_2-TPR profiles can be observed, for all the monometallic catalysts prepared.

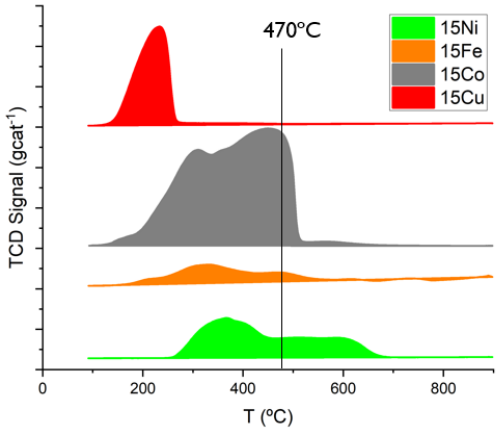

Fig. 1 - H_2-TPR profiles obtained for the monometallic catalysts prepared.

Concerning the profile of the 15Ni catalyst, it can be inferred that the biggest fraction of NiO species was reduced at relatively low temperatures (below 470 °C, which is the temperature used for the reductions prior to the catalytic tests). This is an indicator of the presence of weak interactions between the nickel oxide and the zeolite, indicating that these species might be located on the external surface of the zeolite. [9] The highest peak occurred at approximately 368 °C, which agrees with the literature for the reduction of NiO, whilst situated in the outer layer of the surface of the support CsUSY. In addition, the other peak observed at around 600 °C is related with stronger interactions, formed also between NiO and the zeolite, this time attributed to the reduction of the NiO particles located in the mesoporous cavities of the support.

Regarding 15Cu and 15Co catalysts, it can be observed that their respective metal oxides are mostly reduced below 470 °C.

When consulting the literature for previously developed Fe-zeolite catalysts [10][11], this behavior seems to be common. The reduction peak found at 340 °C could be attributed to the reduction of Fe^{3+} into Fe^{2+} (from Fe_2O_3 into Fe_3O_4). For the temperatures between 400 and 750 °C, the constant reduction peaks noticed can be attributed to the reduction of Fe_3O_4 into Fe°, which may happen through the FeO mechanism (Fe_3O_4 → FeO → Fe°).

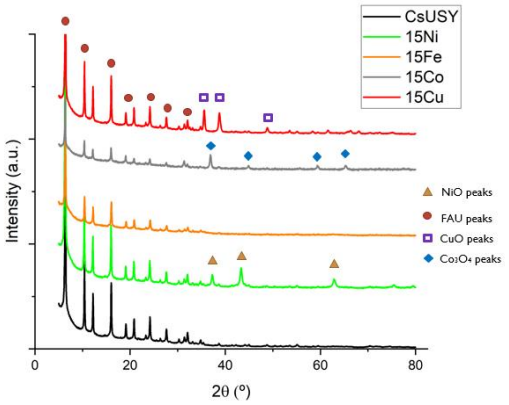

Figure 2 - XRD for the calcined 15X samples.

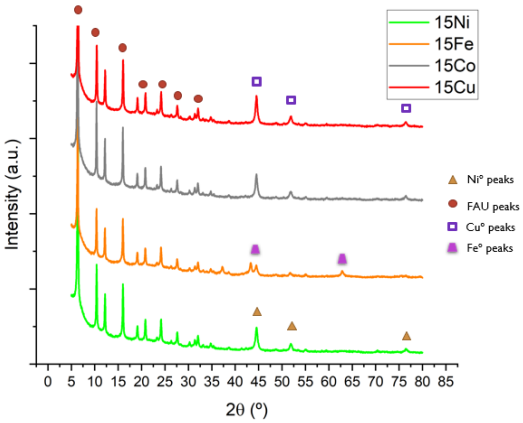

Figure 3 - XRD for the reduced 15X samples.

As can be ascertained by the calcined diffractograms (Fig. 2) the diffraction peaks referring to the faujasite's structure (FAU, red circles) are clearly identifiable in all the catalysts from this study. However in the case of 15Co and 15Fe catalysts, FAU peaks intensity is lower than the found in 15Ni and 15Cu catalysts. This could indicate that the zeolite's crystallinity could be partially affected by the incorporation of these metals. In addition to this, the presence of Ni, Cu and Co oxides is clear in 15Ni, 15Cu and 15Co catalysts, respectively. On the contrary, no iron oxide peaks can be found in 15Fe, suggesting that these species will be highly dispersed over the support. Regarding reduced catalysts patterns (Fig. 3), it is clear the presence of Ni°, Cu° and Co° on $15Ni_{Red}$, $15Cu_{Red}$ and $15Co_{Red}$ catalysts, respectively, while no peaks attributed to Fe° can be clearly found on $15Fe_{Red}$.

As observed in Table 1, Ni and Cu oxides presented similar crystallite sizes, while larger Co oxide crystallites were formed in 15Co catalyst. In the case of 15Fe, the absence of

clearly identifiable peaks did not allow the estimation of the crystallite sizes. Regarding the reduced catalysts properties, the smallest crystallites were found in 15Ni, being remarkable the growth of the crystallites in the case of 15Cu.

Table 1 - Crystallite sizes obtained for the 15X catalysts after calcination and reduction.

Catalysts	d_{Oxide} (nm)	d_{Metal} (nm)
15Ni $15Ni_{Red}$	21 -	- 18
15Fe $15Fe_{Red}$	n.a. -	- n.a.
15Cu $15Cu_{Red}$	21 -	- 47
15Co $15Co_{Red}$	27 -	- 29

As observed in Figure 4, Ni° and Cu° diffraction peaks were found in the catalysts while no remarkable changes were observed in terms of FAU zeolite diffraction peaks. In terms of crystallite sizes, values were similar than those obtained for the reduced catalysts, with variations being <2 nm in all cases. This suggests an absence of remarkable sintering processes during the catalytic tests.

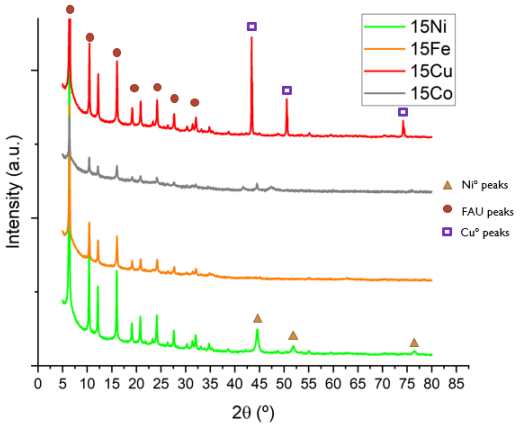

Figure 4 - XRD for the spent 15X samples.

Through the N_2 adsorption isotherms (Fig. 5) it was possible to obtain the textural properties from the 15X samples after calcination, presented in Table X. By analysing the isotherms, all catalysts present the same type of isotherms (with a similar combination of both type I and II, which is characteristic of micro and mesoporous materials). When it comes to the textural properties, it is possible to infer that the addition of any of the metals provoked a reduction on every parameter, when comparing with the CsUSY support, especially when it comes to the external surface area (S_{ext}). This indicates that a greater fraction of metals may be located on the external surface of the zeolite. The reduction of V_{micro}, more remarkable in the case of 15Co, may be related with a partial loss of zeolite's crystallinity or to pores blockage due to the location of metal species. Considering the results previously discussed in terms of XRD, the decrease in the intensity of the zeolite peaks for 15Co together with the reduction of the microporous volume could indicate that the incorporation of cobalt could be responsible for a partial damage of the zeolite structure. On the contrary, the decrease on the intensity of FAU diffraction peaks found for 15Fe could not be attributed to structural damage, as the microporous volume was similar to the obtained for the CsUSY support. Finally, the losses registered on the V_{meso} may be due to the presence of the oxides inside the mesoporous cavities of the zeolite. [3]

Catalyst	**V_{micro} [1] ($cm^3\ g^{-1}$)**	**V_{meso} [2] ($cm^3\ g^{-1}$)**	**S_{ext} [1] ($m^2\ g^{-1}$)**
CsUSY	0.19	0.30	319
15Ni	0.12	0.23	259
15Co	0.08	0.19	182
15Cu	0.13	0.23	229
15Fe	0.18	0.17	164

Table 2 - Textural Properties in the 15X Catalysts.

[1] Micropores volume and external surface area obtained from *t-plot* method;
[2] Mesopores volume obtained as V_{total} (at p/p_0=0.95)-V_{micro}.

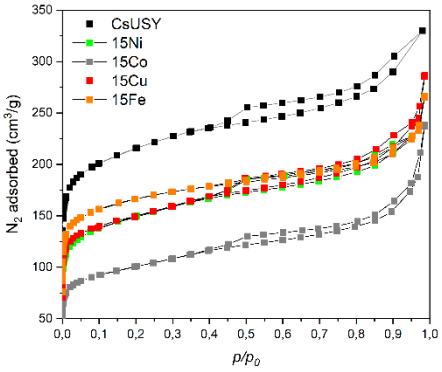

Figure 5 - N_2 Adsorption Isotherms obtained for the support and catalysts of the first study.

The analysis of the reduced 15X catalysts by TEM (Fig. 6) indicated that no metallic Fe nor Cu seems to be clearly found in $15Fe_{Red}$ and $15Cu_{Red}$ catalysts, respectively. In the case of $15Fe_{Red}$, this information is coherent with XRD results, where the presence of diffraction peaks attributed to metallic iron or iron oxides was not clear. On the contrary, metallic particles were

clearly observed in $15Ni_{Red}$ and $15Co_{Red}$ micrographs, being the sizes smaller and more homogeneously distributed in the case of $15Ni_{Red}$ catalyst.

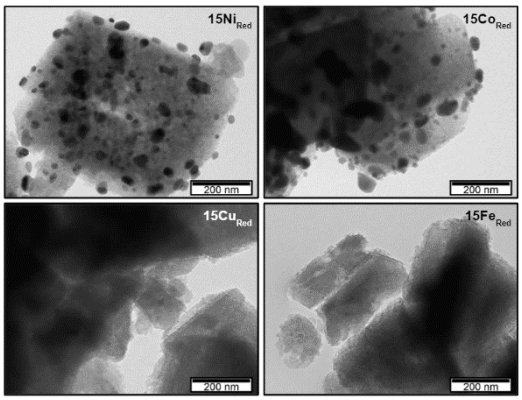

Figure 6 - TEM results for the samples pertaining to the first study.

Catalytic Results – 1st Study

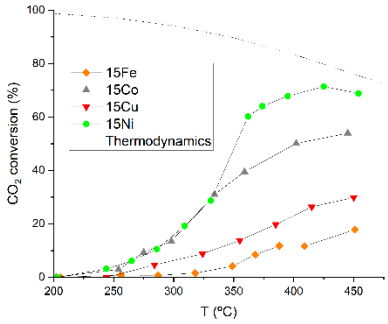

Figure 7 - CO_2 conversion (%) for the 15X catalysts.

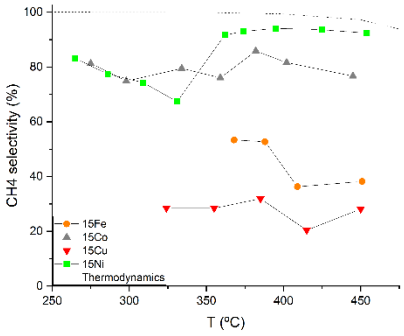

Figure 8 - CH4 Selectivity (%) for the 15X catalysts.

As observed, CO_2 conversions followed the trend: 15Ni > 15Co > 15Cu > 15Fe, while CH_4 selectivity was higher for 15Fe than for 15Cu.

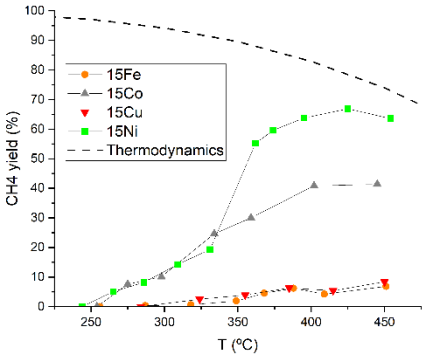

Figure 9 - CH4 Yield (%) for the 15X catalysts.

As observed in Figs. 7, 8 and 9, 15Ni is the most outstanding catalyst, followed by 15Co and with 15Cu and 15Fe leading to similar performances. The higher performance of 15Ni catalyst could be related to this metal being known as more active for the reaction, together with the higher dispersion and smaller particle sizes achieved during the preparation, as already pointed out. For these reasons, in the following studies catalysts based on Ni and doped with low contents (<3 wt%) of a second transition metal were analyzed.

Second Study: Addition of a Second Metal

In terms of H_2-TPR profiles, presented in Figure 10, it can be observed that the most remarkable reduction processes occur below the pre-reduction temperature (470 °C) for the 15Ni1X catalysts. In this way, by comparing the reduction extent below 470 °C, one can clearly observe that the weakest metal-support interactions, inducing reduction processes at lower temperatures, were established on 15Ni1Cu catalyst, followed by 15Ni1Co and, finally, 15Ni1Fe. This suggests that, while in 15Ni1Cu catalyst the oxides will be fully reduced during the pre-treatment, unreduced species will be expectedly present in Co and, especially, Fe-containing samples. The stronger metal-support interactions found in 15Ni1Fe could be responsible for the clear coexistence of NiO and Ni° diffraction peaks in 15Ni1Fe diffractogram.

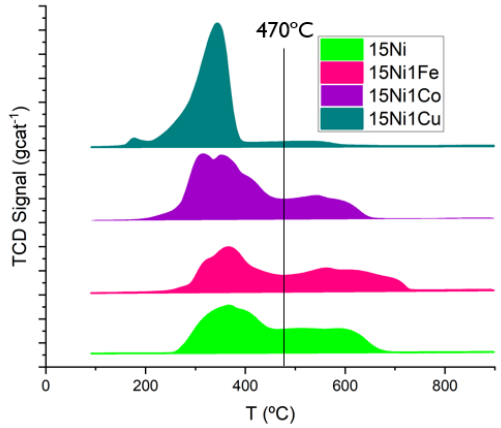

Figure 10 - H_2-TPR profiles obtained for the bimetallic catalysts prepared for the second study.

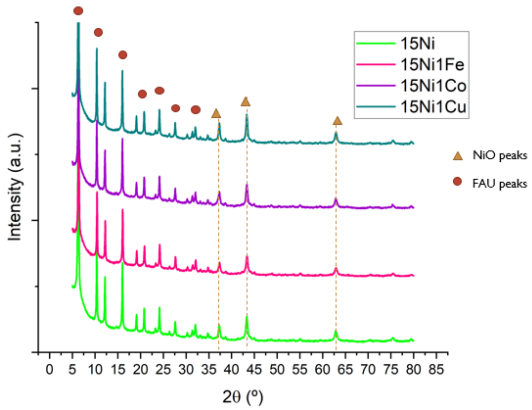

Figure 11 - XRD of the calcined 15Ni1X catalysts.

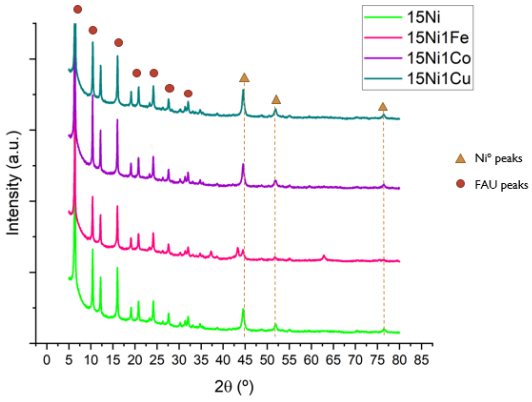

Figure 12 - XRD of the reduced 15Ni1X catalysts.

As can be ascertained by Figure 11, FAU zeolite diffraction peaks can be found in all 15Ni1X catalysts. However, no peaks have been identified for Cu, Fe or Co oxides, which could be due to the low loading incorporated (1 wt%). In addition, NiO and Ni° peaks were found in all calcined and reduced catalysts, respectively. Thus, crystallite sizes were determined and presented in Table. As observed, Cu and Co addition did not induce a positive effect on NiO/Ni° crystallites sizes, while in the case of Fe the interaction of this metal with Ni seems to be responsible for a lower NiO reducibility, being both NiO and Ni° peaks found in this catalyst after reduction at 470 °C. This phenomenon, which did not allow the determination of the average particle size applying Scherrer's equation, could indicate a higher metallic dispersion of nickel in the bimetallic catalyst containing Fe.

Table 3 - NiO and Ni^0 crystallite sizes obtained for the 15Ni1X catalysts after calcination and reduction.

Catalyst	d_{NiO} (nm)	d_{Ni^0} (nm)
15Ni	21	-
15Ni $_{Red}$	-	18
15Ni1Co	21	-
15Ni1Co $_{Red}$	-	19
15Ni1Cu	23	-
15Ni1Cu $_{Red}$	-	19
15Ni1Fe	21	-
15Ni1Fe $_{Red}$	-	n.a.

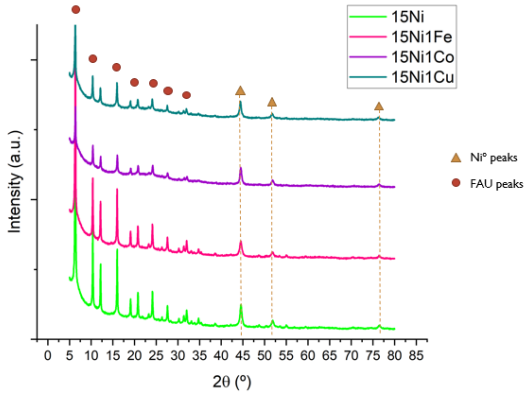

Figure 13 - XRD of the spent 15Ni1X catalysts.

As observed in Figure 13, FAU zeolite peaks can be found in all catalysts, indicating that the structure was preserved during the tests. In addition, the presence of Ni° peaks is clear in all cases, including the 15Ni1Fe samples, which exhibited both NiO and Ni° diffraction peaks after reduction. Thus, this indicates that unreduced NiO species in 15Ni1Fe were fully reduced during the test in presence of hydrogen. By applying Scherrer's equation it was possible to estimate the average Ni° crystallite sizes in spent samples, being the values similar (differences <2 nm) to those found in reduced catalysts. This is indicative of the lack of remarkable sintering processes occurring in the 15Ni and 15Ni1X series during

the catalytic tests. Finally, it must be pointed out that in the case of 15Ni1Fe, for which Scherrer's equation was not applied in the reduced form, the average Ni° crystallite size in the spent catalyst was 16 nm, slightly lower than the obtained for 15Ni (18 nm), 15Ni1Co (20 nm) and 15Ni1Cu (21 nm), confirming the positive impact of Fe in the metallic dispersion.

In terms of hydrophobic character, again characterized by TGA through the calculation of h indexes (Table 4), the incorporation of Cu, Co or Fe to the Ni-catalyst formulation did not lead to remarkable effects. Indeed, it is observed that h indexes are close to 1 (0.93-0.95) in all cases, indicating that all materials are highly hydrophobic.

Table 4 - hydrophobic indexes obtained for 15Ni1X catalysts.

Sample	h index
15Ni	0.95
15Ni1Cu	0.93
15Ni1Co	0.93
15Ni1Fe	0.94

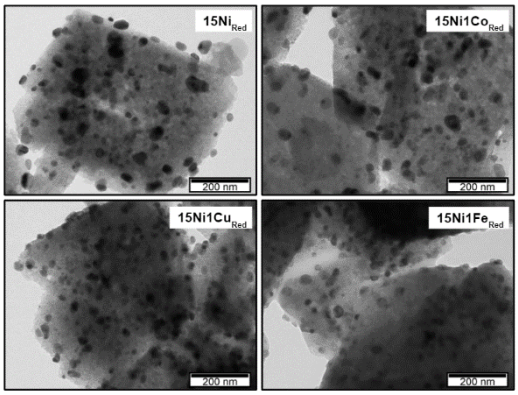

Figure 14 - TEM of the catalysts of the second study.

For TEM microscopy results (Figure 14) the incorporation of a second transition metal seems to induce a better distribution of the Ni° particles over the zeolite, especially when comparing the obtained micrographs with that presented for the monometallic Ni catalyst. In addition, when comparing among the bimetallic series, no remarkable changes in terms of Ni° particle sizes can be observed, in agreement with the crystallite sizes determined from XRD data applying Scherrer's equation. However, the presence of smaller particles can be suggested in 15Ni1Fe.

Catalytic Results

In terms of catalytic performances, in Figures 15 and 16, the incorporation of 1 wt% of Cu induced a significant reduction of the achieved activity. This effect could be due to the weakening of the metal-support interactions (H_2-TPR) and the lack of enhancements in terms Ni^0 particle size (XRD, TEM). Furthermore, Co incorporation, which did not induce changes in the metal-support interactions nor the average Ni^0 particle size, did not report significant changes in terms of performances, being the results similar to those exhibited by the monometallic 15Ni catalyst. Finally, 15Ni1Fe was the catalyst inducing the best performances, with a remarkable improvement of the CO_2 conversion and CH_4 selectivity in the 250 – 380 ºC temperature range. This positive influence derived from Fe addition reveal the existence of potential beneficial synergies between both metals, resulting in stronger metal-support interactions and an enhancement in the dispersion of Ni^0 particles over the zeolite.

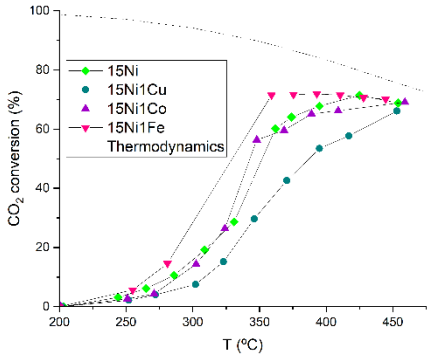

Figure 15 - CO_2 conversion (%) for the 15Ni1X catalysts.

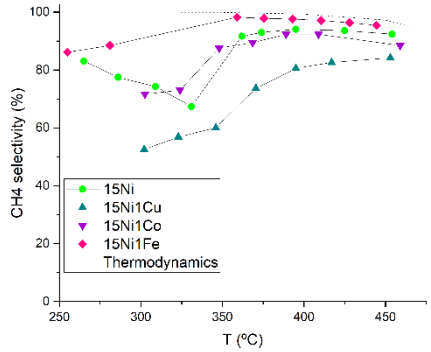

Figure 16 - CH_4 selectivity (%) for the 15Ni1X catalysts.

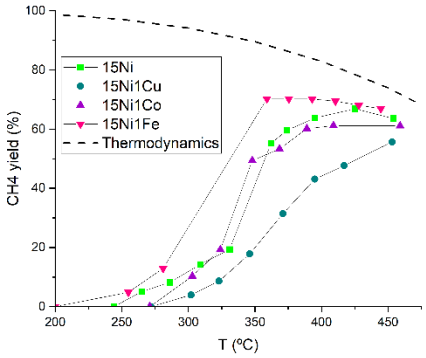

Figure 17 - CH4 yield (%) for the 15Ni1X catalysts.

The presented results follow the order: 15Ni1Fe > 15 Ni ≈ 15Ni1Co > 15Ni1Cu. Since 15Ni1Fe proved to ascertain the best results, this catalyst was used as reference for the third study, and the content of Fe was then varied in order to determine which one would be optimal.

Third Study: Effect of Fe Loading

In terms of reducibility, characterized by H_2-TPR, by observing the profiles presented in Figure 18, it is possible to infer that increasing the Fe loading leads to a displacement of the reduction peaks towards lower temperatures. Consequently, it is expected that the pre-reduction step at 470ºC will lead to a greater presence of metallic species in the catalysts, justifying the absence of NiO diffraction peaks in the patterns of reduced 15Ni2Fe and 15Ni3Fe catalysts, contrary to what found for reduced 15Ni1Fe.

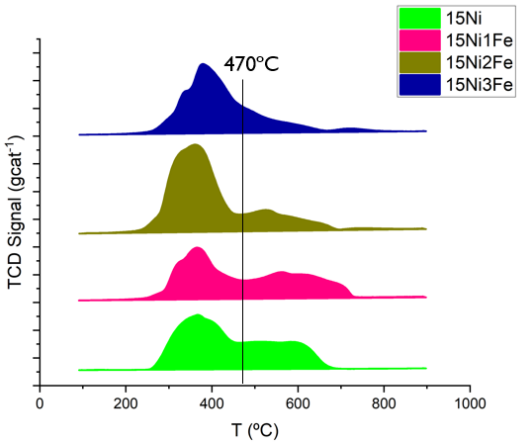

Figure 18 - H_2-TPR profiles obtained for 15NixFe catalysts.

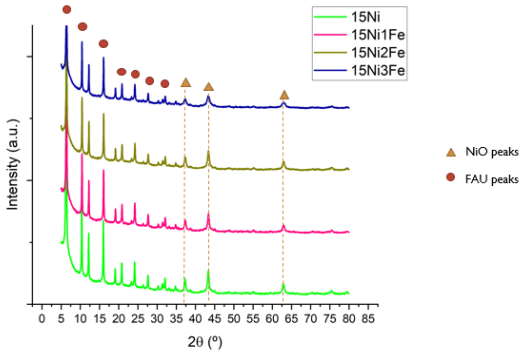

Figure 19 - XRD of the calcined 15NixFe catalysts.

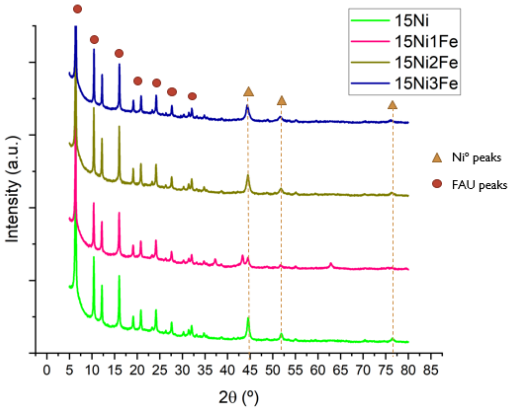

Figure 20 - XRD of the reduced 15NixFe catalysts.

As can be ascertained by the XRD patterns of 15NixFe catalysts exhibited in Figure 19, the variation of the Fe loading did not significantly affect the results. As so, FAU diffraction peaks are clearly observed in all samples, while NiO and Niº diffraction peaks can be found in calcined and reduced catalysts patterns, respectively. In the case of 15Ni1Fe, as previously discussed in this work, both NiO and Niº peaks can be found after reduction, while this behaviour did not occur in the 15Ni2Fe and 15Ni3Fe samples. To be pointed out is that, despite the increase in the incorporated Fe loading, no peaks ascribed to iron oxides could be observed in the samples, which could be related to the low loadings and/or the high dispersion of these species over the support. By applying Scherrer's equation, Niº crystallite sizes were again determined and presented in Table 5. As observed, the increase of Fe loading led to a progressive decrease in NiO and Niº average crystallite sizes, indicating a positive impact of this metal on this parameter.

Table 5 - NiO and Niº crystallite sizes obtained for the 15NixFe catalysts after calcination and reduction.

Catalyst	d_{NiO} (nm)	d_{Ni}^0 (nm)
15Ni	21	-
15Ni $_{Red}$	-	18
15Ni1Fe	21	-
15Ni1Fe $_{Red}$	-	n.a.
15Ni2Fe	16	-
15Ni2Fe $_{Red}$	-	14
15Ni3Fe	12	-
15Ni3Fe $_{Red}$	-	13

As observed in Fig. 21, both FAU zeolite and Niº diffraction peaks can be found in the catalysts, and the determined Niº crystallite sizes were similar (differences <1 nm) to those calculated for reduced catalysts.

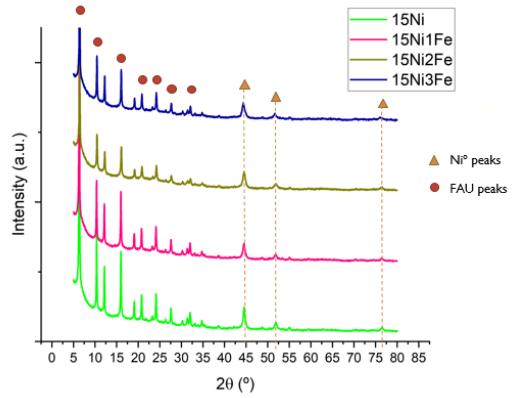

Figure 21 - XRD of the spent 15Ni1xFe catalysts.

In terms of hydrophobic properties (Table 6) the calculated h indexes reveal that all Fe-containing catalysts present weak interactions with water molecules (h indexes > 0.90 in all cases). However, the increase of Fe loading seems to lead to a more hydrophilic character, as the h index presented by 15Ni3Fe is the lowest from the series.

Table 6 - Hydrophobic indexes obtained for 15NixFe catalysts.

Sample	h index
15Ni	0.95
15Ni1Fe	0.94
15Ni2Fe	0.95
15Ni3Fe	0.92

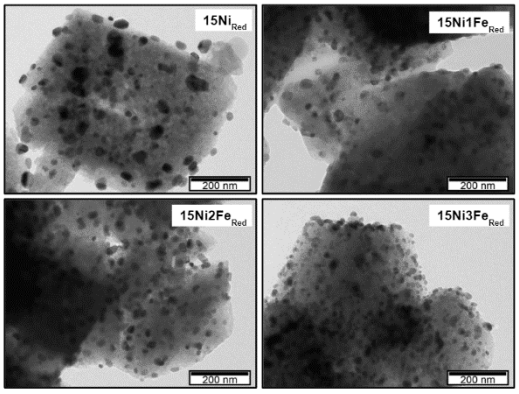

Figure 22 - TEM images obtained for the catalysts of the third study.

TEM micrographs were also collected for 15NixFe catalysts after reduction at 470 ºC (Figure 22). As observed, the increase of the iron content appears to reduce the particle sizes of Niº, in accordance with XRD results previously discussed. In addition, a more homogeneous distribution of Niº particles is observed for higher Fe loadings, especially when comparing with the monometallic 15Ni.

Catalytic Tests

Concerning the influence of Fe loading in the catalytic performances of 15NixFe samples, shown in Figures 23 and 24, it is clear that all Fe-containing catalysts exhibit higher methane selectivity than 15Ni. In terms of CO_2 conversion, increasing Fe loading leads to a reduction of the activity. Despite the reduction in the Niº particle sizes with the addition of increasing Fe loadings, the lack of catalytic enhancements in 2 and 3 wt% Fe samples could be due to the weakening of the metal-support interactions verified by H_2-TPR. To be pointed out is the activity tendency below 350 ºC. Indeed, in this region 15Ni2Fe catalyst exhibited the best results. On the contrary, for temperatures above 350 ºC, 15Ni1Fe sample portrays the most active catalyst. This could indicate that the metal-support interactions could present a predominant role at higher temperatures, while the metallic dispersion could be more relevant at lower temperatures. In the case of 15Ni3Fe, despite the lower Niº particle size, the slightly lower hydrophobicity and weaker metal-support interactions could be in the origin of the displayed performances.

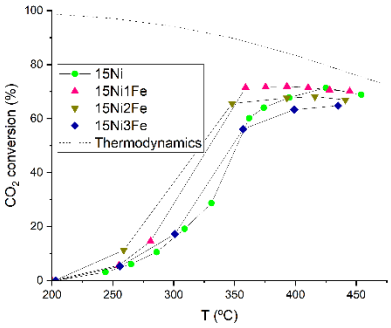

Figure 23 - CO_2 conversion (%) for the 15Ni1xFe catalysts.

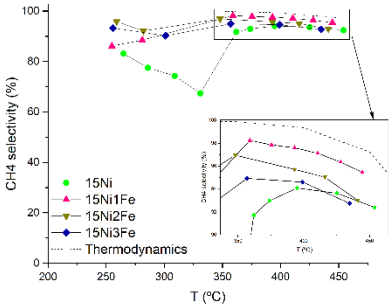

Figure 24 – CH_4 selectivity (%) for the 15NixFe catalysts.

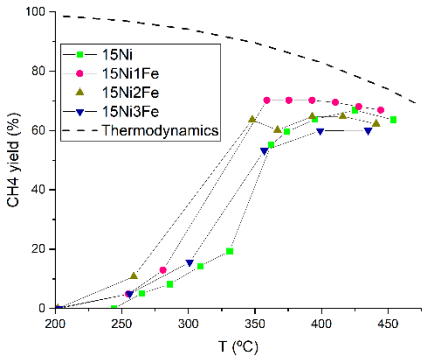

Figure 25 - CH_4 yield (%) for the 15NixFe catalysts.

Despite the lower reducibility of the metal oxides below 470 ºC, 15Ni1Fe obtained the best results, suggesting the establishment of promising synergies between iron and the nickel species in this sample. In addition, the lack of results for this sample in the range of temperature of 280 and 360 ºC is due to the fact that since the reaction is exothermic, the high conversion rate in this region results in an overheating of the catalytic bed, precluding the temperature measurement in between that specific range.

Conclusion

The conversion of carbon dioxide into methane is a promising alternative for natural gas obtained through fossil fuels.

Through the first study of the series, nickel proved to be the most active metal on itself, which was attributed to its well-known suitability towards carbon dioxide methanation and favoured metallic dispersion. On the second study, 15Ni1Fe exhibited the highest performances, which was attributed to the establishment of proper synergies between the metals, improving the metal-support interactions and favouring the metallic dispersion. In the third study, it was concluded that both 15Ni1Fe and 15Ni2Fe had their own set of temperature range for which they were the most outstanding materials. However, the use of lower Fe loadings was found as more suitable, which was attributed to a slight reduction of the catalysts hydrophobicity and weakening of the metal-support interactions with higher Fe contents.

Citations

1. I. Graça, L.V. González, M.C. Bacariza, A. Fernandes, C. Henriques, J.M. Lopes, M.F. Ribeiro. *CO2 hydrogenation into CH4 on NiHNaUSY zeolites.* Applied Catalysis B: Environmental 2014 101-110.
2. Bacariza, C. (2018). *CO_2 conversion to CH_4 using metallic catalysts supported on zeolites* [Doctoral dissertation, Instituto Superior Técnico].
3. M. Bacariza, S.Amjad, P. Teixeira, J. Lopes, C. Henriques. *Boosting Ni Dispersion on Zeolite-Supported Catalysts for CO2 Methanation: The Influence of the Impregnation Solvent*. Energy & Fuels, 34, 11, 14656-14666, 2020.
4. Bill Gates. *How to Avoid a Climate Disaster*. Alfred A. Knopf, february 2021
5. *Climate Change 2014: Synthesis Report. Contribution of Working*. Groups I, II and III to the Fifth Assessment Report of the Intergovernmental. Panel on Climate Change. Core Writing Team, Pachauri, R.K., Meyer, L.A., Eds.; IPCC: Geneva, Switzerland, 2014.
6. Westermann A., Azambre B., Bacariza M.C., Graça I., Ribeiro M.F., Lopes J.M., Henriques C. (2015). *Insight into CO2methanation mechanism over NiUSY zeolites: Anoperando IR study*. Appl Catal Environ B 174–175, 120–125
7. Tsiotsias, A.I.; Charisiou, N.D.; Yentekakis, I.V.; Goula, M.A. *Bimetallic Ni-Based Catalysts for CO2 Methanation: A Review*. Nanomaterials 2021, 11, 28.
8. C. Vogt, M. Monai, E. B. Sterk, J. Palle, A. E.M. Melcherts, B. Zijlstra, E. Groeneveld, P. H. Berben, J. M. Boereboom, E. J. M. Hensen, F. Meirer, I. A. W. Filot, B. M. Weckhuysen. *Understanding carbon dioxide activation and carbon–carbon coupling over nickel*. Nature Communications (2019) 10:5330
9. Z. Zhang et al., "Regulation the reaction intermediates in methanation reactions via modification of nickel catalysts with strong base," Fuel, vol. 237, no. October 2018, pp. 566–579, Feb. 2019.